Post-transcriptional regulation of aortic calcification in KLOTHO deficient mice: impact of miR-145 and miR-378

Ying Tang, Tapan A. Shah[*], Diane E. Garsetti, and Melissa B. Rogers[#]

Rutgers - New Jersey Medical School, Microbiology, Biochemistry, & Molecular Genetics, Newark, NJ

Running title: MicroRNA profiles in calcified *vs*. healthy aorta

*Present Address: Advanced Cell Diagnostics, 7707 Gateway Blvd #200, Newark, CA 94560

#To whom should correspondence and reprint request be addressed to: Melissa B. Rogers, Ph.D., Microbiology, Biochemistry & Molecular Genetics, Rutgers - NJ Medical School, Center for Cell Signaling, Room F1216, 205 South Orange Ave., Newark, NJ 07103. Email: rogersmb@njms.rutgers.edu, telephone: 973 972 2984

Keywords: BMP, Klotho, SMAD transcription factor, gene regulation, signaling, cardiovascular, calcification, atherosclerosis, renal physiology

Grant Support: Funding was provided by the National Heart, Lung, and Blood Institute R01HL114751 and National Institutes of Aging R56AG050762 to MBR

Conflict of Interests Disclosure: The authors declare that they have no conflicts of interest with the contents of this article.

Abstract

Atherosclerosis and calcific aortic valve disease are common in the aged as well as in those with kidney disease, diabetes, and high cholesterol. Although cardiovascular calcification is a major pathological feature, calcific molecular mechanisms are poorly understood. High bone morphogenetic protein 2 (BMP2) levels and BMP signaling promote calcification. We sought to identify and restore mechanisms that restrain BMP signaling in healthy cardiovascular tissue. The 3' untranslated region (3'UTR) of the *Bmp2* transcript restrains BMP2 synthesis in healthy aorta, valves, and vasculature by mechanisms that are conserved between rodents and humans. MicroRNAs (miRNAs) post-transcriptionally modulate gene expression *via* the 3'UTR and have clinical potential as biomarkers and therapeutic agents. Our goal is to elucidate the role of miRNAs during pathological calcification in the *Klotho* mouse model of kidney disease. We generated abundance profiles of miRNAs that normally repress BMP2 and other pro-osteogenic proteins in healthy and calcified mouse aorta. We also demonstrated that restoring normal levels of the miR-145 and miR-378 miRNAs can repress the synthesis of BMP2 and other pro-osteogenic proteins and inhibit pathological calcification *in vivo*. These miRNAs are candidates for "miRNA replacement therapies" in the context of chronic kidney disease.

Introduction

The American Heart Association projects that 45% of Americans will have some form of heart and/or vascular disease by 2035 (1). Calcification of blood vessels reduces their diameter and plasticity and ultimately promotes ischemic events (2). Risk factors that promote both vascular and valvular calcification include aging, renal failure, and male sex; as well as hypercholesterolemia, smoking, and diabetes (3,4). An aging population and the epidemic of obesity ensure that cardiovascular disorders will be a major public health threat for decades to come. Understanding the signaling processes that regulate the behavior of vascular cells will reveal novel approaches to preventing and treating these devastating pathologies.

The molecular mechanisms underlying vascular calcification have been widely studied. Abnormally elevated levels of the pro-osteogenic bone morphogenetic protein 2 (BMP2) and increased BMP signaling are implicated in all forms of pathological cardiovascular calcification. For example, BMP2 is synthesized in human atherosclerotic plaques (5) and calcified stenotic valves (6). Moreover, BMP2 can induce master osteogenic factors such as RUNX2 in human aortic valve interstitial cells (7) and MSX2 in aortic smooth muscle cells (8), induce calcification *in vitro* (7,9-12), and cause ossification within adult diseased valves (12-14) and atherosclerotic plaques (5). Forced synthesis of BMP2 in vascular smooth muscle cells accelerated atherosclerotic calcification in *ApoE* null mice fed a high cholesterol diet (15). Genetic deficiency and pharmacological inactivation of BMP signaling reduced calcification not only in cultured cells (12,16,17) but also in *Ldlr* null mice fed a high-fat diet (18), *Mgp* null mice (19) and *Klotho* mutant mice with renal failure (16).

Given the importance of BMP2 and BMP signaling in cardiovascular calcification, identifying post-transcriptional regulators of BMP2 expression may provide new insights and targets for the treatment of cardiovascular disease. The 3'-untranslated region (3'-UTR) binds regulatory proteins and microRNAs (miRNAs) that influence polyadenylation, translation efficiency, and stability of mRNAs (20). The length and extreme evolutionary conservation of the *Bmp2* 3'-UTR supports a major role for post-transcriptional regulation involving miRNAs (21-23)}. The goal of this study was to compare the profiles of miRNAs that modulate the synthesis of BMP2 and downstream BMP signaling proteins in the aorta of healthy mice relative to mice with pathologically calcified aorta. Our mouse model is a *Klotho* hypomorph that causes dysregulated mineral metabolism (24).

Mice homozygous for *Klotho* mutations have a short lifespan, growth retardation, osteoporosis, atherosclerosis, ectopic calcification, and renal disease. The KLOTHO protein, along with $1,25(OH)_2$ vitamin D3 and FGF23, tightly regulates phosphate homeostasis (25,26). Deficiency of KLOTHO leads to renal disease and subsequent hyperphosphatemia and ectopic calcification of soft tissues such as aorta, aortic valves and kidneys (16,26). Restoration of normal KLOTHO levels ameliorates calcification (25). The dramatic calcification of the aorta and other tissues in *Klotho* mutant mice within 6-7 weeks of birth make them experimentally attractive for studying the regulation of the *Bmp2* gene during pathological calcification. Furthermore, understanding the mechanism of aortic calcification in the context of kidney failure is important because 17% of the population over the age of 30 may suffer from this major cardiovascular disease risk factor by 2030 (1).

Our objective was to elucidate a comprehensive profile of miRNAs whose abundance is altered in the calcified aorta of *Klotho* homozygous mutant mice with renal disease. We also demonstrate that selected miRNAs can modulate the BMP2 ligand and proteins involved in BMP signaling and calcification *in vivo*. This study begins to fill a key gap in our understanding of post-transcriptional processes that control BMP signaling and calcification in vascular tissues and provides experimental support for miRNA replacement therapies in cardiovascular disease.

Materials and Methods

Tissue sample collection for microRNA microarray

Mice bearing the *Klotho* mutation were a gracious gift from Dr. Makoto Kuro-o (Jichi Medical University) by way of Dr. Sylvia Christakos (Rutgers New Jersey Medical School). The mice were a mixture of strains FVB, C57Bl/6J, and C3H/J. Because homozygous *Klotho* null mice are infertile, mice were maintained by heterozygous-by-heterozygous mating. 25% of each litter was homozygous and exhibited the full *Klotho* phenotype, including ectopic soft tissue calcification. 50% were heterozygous and 25% were wild type. No statistically significant differences in any parameter were observed between mice bearing the heterozygous and wild type *Klotho* genotypes. Assessed parameters included the body and organ weights, gene expression, and calcium levels (27,28). Because our analyses were consistent with published data indicating that the *Klotho* mutation is fully recessive, heterozygous and wild type samples are presented together as “healthy control” samples.

All animal procedures were in accordance with the guidelines for Care and Use of Experimental Animals and approved by the NJ Medical School Institutional Animal Care and Use Committee (IACUC protocol #PROTO999900898). Control and *Klotho* homozygote mice were fed regular chow and euthanized at 51 ± 3.4 days of age. After weaning, *Klotho* homozygotes received softened chow on the floor of the cage. On the day of necropsy, mice were killed with an inhalation overdose of isoflurane. Immediately thereafter, the heart was perfused *via* the left ventricle with phosphate buffered saline (PBS, pH 7.3), to remove excess blood. The aorta including the ascending aorta, arch and descending thoracic aorta was removed. After cutting at the surface of the heart, the aorta was rinsed in PBS, blot dried and weighed. The aorta was snap-frozen in liquid nitrogen and stored at -80°C. Frozen tissues were ground in liquid nitrogen using a mortar and pestle. RNA was extracted using the miRNeasy Mini Kit (Qiagen Inc., Germantown, MD, # 217004). The RNA quality was checked using Bioanalyzer (Agilent Technologies, Santa Clara, CA).

Calcium assays

Aorta tissues were ground in liquid nitrogen using a mortar and pestle and lysed by sonication on ice in PBS, pH 7.3, containing 0.16 mg/mL heparin. The Cayman Chemical Calcium Assay kit (Ann-Arbor, MI, #701220) was used to measure calcium levels. Calcium levels were normalized to protein levels measured using the Pierce BCA Protein Assay Kit (ThermoFisher Scientific, Waltham, MA, #23225).

MicroRNA microarray and data analysis

Aortic samples were obtained from both male and female control and *Klotho* mutant mice (Table 1). MicroRNA expression in the aorta was assessed with the Applied

Biosystems™ GeneChip™ miRNA 4.0 Array (ThermoFisher Scientific, Waltham, MA, #902412) in the Rutgers NJMS Genomics Center. The GeneChip™ miRNA 4.0 Array contained the miRNAs and pre-miRNAs (precursors to the miRNAs) listed in the Sanger miRBase v20. The miRNA arrays were processed following the manufacturer's instructions. Briefly, using the Applied Biosystems™ FlashTag™ Biotin HSR RNA Labeling Kit (ThermoFisher Scientific, Waltham, MA, the # 902446), 400 ng of total RNA was labeled with biotin and hybridized to the miRNA 4.0 Array (ThermoFisher Scientific, Waltham, MA, #902412) for 18 hours at 48°C using an Affymetrix® 450 Hybridization Oven (Affymetrix, Santa Clara, CA). After washing and staining on an Affymetrix® 450 Fluidics Station (Affymetrix, Santa Clara, CA), using the Applied Biosystems™ GeneChip™ Hybridization, Wash, and Stain Kit (ThermoFisher Scientific, Waltham, MA, #900720), the arrays were scanned using the Affymetrix® Scanner 3000 7G (Affymetrix, Santa Clara, CA). CEL files were generated using the Affymetrix data extraction protocol in the Affymetrix GeneChip® Command Console® Software (Affymetrix, Santa Clara, CA, USA). The resulting CEL files (GSE135759) were analyzed using the Partek Genomics Suite 7.0 (Partek Inc., St. Louis, MO), including the Robust-Multi-array Average algorithm to correct for microarray background and to normalize miRNA expression profiles on a log scale. Partek Genomic's ANOVA analysis identified the miRNAs whose abundance differed significantly between control and *Klotho* homozygous mutant mice. Minimal significance was defined as a p value of 0.05.

Table 1. Number of mice (n) used for the miRNA profiling

	Males		**Females**	
Group	**Age**	**n**	**Age**	**n**
Control (Wt)	7-8 weeks	5	7-8 weeks	4
Control (K+)	7-8 weeks	2	7-8 weeks	1
Klotho mutant (KK)	7-8 weeks	5	7-8 weeks	2

Biological process analyses

MicroRNAs that differed significantly in *Klotho* mice compared to control were further divided by sex into sets of significantly up- or down-regulated miRNAs (see microarray data analysis). Predicted target profiles of differentially expressed miRNAs were determined by DNA Intelligent Analysis (DIANA)-micro T-CDS (v. 5.0) (http://www.microrna.gr/webServer) which permits the entry of multiple miRNAs simultaneously (29). The micro T-CDS threshold score for predicted targets was set at 0.7. Scores ranged from 0 to 1, with a higher score indicating an increased probability of a true microRNA target. To classify and visualize the biological processes affected by target genes, Gene Ontology (GO) and KEGG (Kyoto Encyclopedia of Genes and Genomes) were utilized with the R package, clusterProfiler (http://bioconductor.org/packages/release/bioc/html/clusterProfiler.html) (30). Minimal significance was defined as a *p* value of 0.05.

MicroRNA-BMP signaling network analyses

The miRNAs that may affect the ligand BMP2 and the canonical signaling proteins SMAD1, 5, and 9 were determined using DIANA-micro T-CDS (v. 5.0), TargetScan (http://www.targetscan.org/vert_72/), and miRanda (31) computational prediction tools. Our analyses were focused on the miRNAs that were down-regulated in *Klotho* mutant mice and predicted to affect the ligand BMP2 and the BMP-specific SMADs . Cytoscape software (32) was used to construct the interaction network between miRNAs and BMP signaling.

Real-Time PCR for detection of microRNA-145 and microRNA-378a and target gene expression

MicroRNA cDNA was synthesized using the miScript PCR Kit (Qiagen Inc., Germantown, MD, # 218073). The miScript PCR kit utilized a universal oligo-dT primer tag to convert all RNA species (total RNA and miRNA) into cDNA. A universal reverse primer supplied with the miScript PCR kit was used to amplify cDNA from each miRNA. The miRNA forward primers were designed based on miRNA sequences in miRBase 22 (http://www.mirbase.org/). GCG or CGC was added to the 5' end of the primers when the GC % was low. NCBI nucleotide blast was used to confirm the absence of non-specific binding sites for the forward primers. Messenger RNA (mRNA) cDNA was synthesized using the QuantiTect® Reverse Transcription kit (Qiagen Inc., Germantown, MD, # 205313). Intron-spanning primers for mRNA were used to eliminate amplicons generated from any contaminating genomic DNA. Primer sequences are shown in Table 2.

Quantitative PCR was performed on a CFX96 Touch™ Real-Time PCR Detection System (Bio-Rad Laboratories, Hercules, CA, #1855196) using the QuantiTect® SYBR® Green PCR kit (Qiagen Inc., Germantown, MD, #204145) under the following conditions: 15 min at 95°C, 39 cycles of 15 seconds at 94°C, 30 seconds at 55°C and 30 seconds 70°C. MicroRNA abundance was normalized to U6 and mRNA expression was normalized to actin. The human U6 primer used in this experiment was included in the miScript Primer assay kit (Qiagen Inc., Germantown, MD, #218300).

Table 2. Real-Time PCR primer sequences

Name	**Primer Sequence (5'-3')**
mmu-miR-145a-3p	F: GCGATTCCTGGAAATACTGTTCTTG
mmu-miR-145a-5p	F: GTCCAGTTTTCCCAGGAATCCCT
mmu-miR-378a-5p	F: CTCCTGACTCCAGGTCCTGTGT
Mouse *Bmp2*	F: TAGATCTGTACCGCAGGCA R: GTTCCTCCACGGCTTCTTC
Mouse *Smad1*	F: GTGTATGAACTCACCAAAATGTGC R: TAACATCCTGCCGGTGGTATTC
Mouse *Smad5*	F: AACTTTCACCATGGCTTCCA R: CCAGAAGCTGAGCAAACTCC
Mouse *β-actin*	F: CGCCACCAGTTCGCCATGGA R: TACAGCCCGGGGAGCATCGT

Lentiviral microRNA-145 and microRNA-378a transduction

A lentivirus vector expressing mir-145 or mir-378a under the control of the vascular smooth muscle cell (VSMC)-specific mSm22a promoter was purchased from Biosettia (Biosettia Inc, San Diego, CA). The negative control was the empty virus vector. Newly weaned *Klotho* mutant homozygotes were injected with empty lentivirus or lentivirus

bearing mir-145 or mir-378a *via* their tail veins on 5 alternate days. The total lentivirus achieved in each mouse at the end of the treatment window was 4×10^5 pfu/g body weight. The mir-145 lentivirus generates two mature miRNAs: miR-145a-5p and miR-145a-3p. The mir-378a lentivirus generates two mature miRNAs: miR-378a-5p and miR-378a-3p.

Statistical Analysis

Data are presented as mean ± SEM and analyzed with GraphPad (version 7; GraphPad Software Inc, La Jolla, CA). Statistical significance was assessed with either the Student's two-tailed t-test or ANOVA. Differences were considered significant at $p<0.05$.

Results

MicroRNA profiles differ in the aorta from *Klotho* mice

MicroRNAs are crucial regulators in cardiovascular pathologies (33). Consequently, we hypothesized that miRNA profiles differ in aorta from healthy control mice and *Klotho* homozygous mutant mice with renal disease. BMP signaling and calcium levels are doubled in the aorta of Klotho homozygotes (27,28). To identify miRNAs involved in aortic calcification, we profiled miRNAs in aortas from control healthy and *Klotho* mutant mice. In total, 135 miRNAs were significantly increased and 77 miRNAs were significantly decreased in *Klotho* mutant homozygous males relative to control mice ($p<0.05$, Fig. 1ATable 3). In *Klotho* mutant females, 62 miRNAs were significantly increased and 88 miRNAs were significantly decreased ($p<0.05$, Fig. 1B, Table 3). These results are consistent with a major role for miRNA-mediated post-transcriptional regulation in aortic calcification.

Table 3. The number of miRNAs that differed in control relative to *Klotho* mice

	Male	Female
Any significant change, p<0.05		
Increased in KK vs CTR	135 (7.1%)	62 (3.3%)
Reduced in KK vs CTR	77 (4.0%)	88 (4.6%)
1.5-fold difference, p<0.05		
Increased in KK vs CTR	88 (4.6%)	21 (1.1%)
Reduced in KK vs CTR	44 (2.3%)	57 (3.0%)
2-fold difference, p<0.05		
Increased in KK vs CTR	64 (3.4%)	11 (0.6%)
Reduced in KK vs CTR	29 (1.5%)	29 (1.5%)

Differentially expressed miRNAs in *Klotho* mutant mice target osteogenic differentiation

MicroRNAs influence many biological processes in vascular cells (33). We hypothesized that miRNAs that are differentially expressed in the calcified aortas of *Klotho* mutant mice may affect processes related to osteogenesis. We used GO terms and the KEGG pathway to computationally predict the biological processes potentially regulated by the miRNAs whose abundance was altered in *Klotho* mice relative to control mice. Consistent with a role in vascular calcification, biological processes relevant to osteogenic differentiation (4,34) such as skeletal development and the WNT and HIPPO signaling pathways were predicted to be targeted by the differentially regulated miRNAs (Fig. 2A-D, Supporting Fig. 1A-D).

Down-regulated miRNAs target BMP signaling

The BMP signaling pathway is essential for osteogenesis and vascular calcification (4,34,35). BMP2 binds to the BMP receptor (BMPR), which phosphorylates and activates SMAD signaling. SMAD signaling increases transcription of RUNX2 and MSX2, leading to increased osteogenic differentiation (4,34,36). We hypothesized that miRNAs that repress *Bmp2* and *Smad1, 5 and 9* might be down-regulated in the *Klotho* mice. Down-regulation of miRNAs that repress ligands and signaling mediators would partly account for the elevated BMP signaling observed in the *Klotho* aorta (27,34)). To visualize potential target relationships between down-regulated miRNAs in *Klotho* mutant mice and *Bmp2* and *Smad1, 5* and *9* protein coding transcripts, we employed the open source software Cytoscape. MiR-717 was significantly down-regulated in male *Klotho* mutant mice (84% of control levels, Supporting Table 1, Fig. 3) and was predicted to target all four genes (Fig. 3). Among the miRNAs down-regulated significantly in female *Klotho* mutant mice, miR-7235-3p and miR-7685-3p may target all four genes. The abundances of these two miRNAs were 76% and 84% of control levels, respectively (Supporting Table 1). The Cytoscape network showed that nine miRNAs were notable because they were significantly decreased in both male and female *Klotho* mutant mice and also may target *Bmp2* and/or *Smad1, 5, or 9*. These were miR-182-5p, miR-30e-5p, miR-187-5p, miR-378a-5p, miR-3065-5p, miR-708-5p, miR-193a-3p, miR-193b-3p and miR-193b-5p (Table 4). We postulate that microRNAs that target more than one member of the BMP signaling pathway may inhibit BMP signaling by coordinately down-regulating multiple proteins and effectively restrain pathological calcification.

Table 4. Relative abundance of miRNAs down-regulated in both male and female *Klotho* mice

Name	% control in males	% control in females
miR-182-5p	46	50
miR-30e-5p	49	55
miR-187-5p	42	27
miR-378a-5p	55	37
miR-3065-5p	65	80
miR-708-5p	52	61
miR-193a-3p	48	30
miR-193b-3p	52	27
miR-193b-5p	55	15

MicroRNA-145 and microRNA-378a attenuation in *Klotho* mutant mice

We selected two microRNAs to test the principle that an miRNA targeting several members of the BMP signaling pathway would reduce KLOTHO deficiency-associated calcification. The vascular regulator miR-145a is predicted to target *Bmp2*, *Smad1* and *Smad5* (Table 5, (37)) and to improve atherosclerotic symptoms in a mouse model of hyperlipidemia (38). Our microarray measurements showed that the abundance of miR-145a-5p was reduced by 25% in male *Klotho* mice as compared to healthy control mice (Fig. 4A, Supporting Table 1). RT-PCR indicated that levels of both miR-145a-5p and -3p were signficantly reduced in *Klotho* mutant mice (Fig. 4B, D). The experiments described below test the impact of increasing miR-145 abundance in the setting of kidney failure and accelerated aging.

The abundance of another microRNA predicted to target both *Bmp2* and *Smad5*, miR-378a-5p, was sharply decreased in both male and female *Klotho* mutant mice (54% and 37% respectively, Fig. 4E). The circulating level of miR-378 also was reduced in the plasma of patients with coronary heart disease (1). Recent studies confirmed the expectation (Table 5) that miR-378 directly regulates *Bmp2* (39,40). RT-PCR validated our microarray results and confirmed that the abundance of miR-378a-5p in *Klotho* mutant mice was half that present in healthy control aorta from both sexes (Fig. 4F).

Table 5. Sequence alignments between miR-145a-5p, miR-145a-3p and miR-378a-5p and mRNAs encoding BMP signaling proteins

Position 3133-3141 of **Bmp2** 3' UTR	5′...GGGAAUAAUUAGGAAAACUGUGAC...
	| || | |||||||| ||
mmu-miR-145a-5p	3′ UCCCUAAGGACCCUUUUGAC-CUG
Position 2882-2889 of **Bmp2** 3' UTR	5′...UCAUCAGGAAUGCCUCCAGGAAA...
	|||||||
mmu-miR-145a-3p	3′ GUUCUUGUCAUAAAGGUCCUUA
Position 1203-1209 of **SMAD1** 3' UTR	5′...GCAGGGUUUUUCUCUACUGGAAA
	||||||
mmu-miR-145a-5p	3′ UCCCUAAGGACCCUUUUGACCUG
Position 249-256 of **SMAD5** 3' UTR	5'...UUAGCAUUGAUCUUAAACUGGAA...
	|||||||
mmu-miR-145a-5p	3' UCCCUAAGGACCCUUUUGACCUG
Position 568-574 of **Bmp2** 3' UTR	5'...UAUAUUCUUCAAUUCUCAGGAAU...
	||||||
mmu-miR-378a-5p	3' UGUGUCCUGGACCUCAGUCCUC
Position 738-745 of **Bmp2** 3' UTR	5'...GAAAACUGUGACUAUGUCAGGAA...
	|||||||
mmu-miR-378a-5p	3' UGUGUCCUGGACCUCAGUCCUC
Position 2870-2876 of **Bmp2** 3' UTR	5'...CGGGCACCUCAGUCAUCAGGAAU...
	||||||
mmu-miR-378a-5p	3' UGUGUCCUGGACCUCAGUCCUC
Position 1172-1178 of **SMAD5** 3' UTR	5'...UUUACUUGGCAGCCUUCAGGAAC...
	||||||
mmu-miR-378a-5p	3' UGUGUCCUGGACCUCAGUCCUC

Forced overexpression of mir-145 and mir-378a levels in *Klotho* mutant mice

We used a vascular smooth muscle cell (VSMC)-specific *mSm22a* promoter-driven lentivirus to increase the abundance of miR-145 and miR-378a in the aortas of *Klotho* mutant homozygotes (Fig. 5A). To evaluate the efficacies and persistence of lentiviral transduction, RT-PCR was used to test the aortic levels of miR-145 and miR-378a in mice injected with viruses bearing these miRNAs relative to empty virus vectors. The

miR-145 virus raised miR-145a-5p and miR-145a-3p abundances by 1.4±0.8 and 2.0±0.01 fold, respectively, relative to empty virus (Fig. 5B, C). Similarly, miR-378a-5p abundance increased by 1.7±0.04 fold (Fig. 5D). Thus this delivery dosage and method successfully augmented aortic miR-145 and miR-378a levels in *Klotho* mutant mice.

Increased expression of miR-145 and miR-378a reduced BMP signaling and aortic calcification

Three different proteins involved in BMP signaling: BMP2 and SMAD1 and 5 are predicted to be targeted by miR-145 (Table 5). Therefore, we hypothesized that increased miR-145 levels would repress the synthesis of these pro-osteogenesis factors and ameliorate pathological calcification. Having successfully augmented the level of miR-145 with lentivirus delivery, we evaluated the impact of this treatment on *Bmp2* and *Smad1* and *5* RNA levels with RT-PCR. The *Bmp2* and *Smad5* RNA levels in aortas from mice injected with miR-145-bearing virus fell to 48±0.03% and 65±0.006% ($p = 0.05$) that of control aortas from mice injected with empty virus (Fig. 6A, C). The miR-145 virus did not significantly change the abundances of the *Smad1* RNA (Fig. 6B).

To test if miR-145 overexpression inhibited pathological calcification in *Klotho* mice, we compared the calcium present in the aortas of *Klotho* mice injected with empty lentivirus vector or with virus bearing miR-145. The *Klotho* mice injected with the miR-145 virus had one third less aortic calcium as that observed in the empty virus injected mice (67±0.8%, $p = 0.002$, Fig. 6). Thus, forced miR-145 expression limited pathological calcification in *Klotho* aorta.

The down-regulated miR-378a miRNA is predicted to target *Bmp2* and *Smad5* (Fig. 3, 4). To evaluate the potiential benefit of restoring miR-378a expression in the aorta of

Klotho mutant mice, a lentivirus bearing miR-378a was injected. This virus reduced the levels of the target gene RNAs *Bmp2* and *Smad5* to 60±0.02% (p =0.02) and 64±0.4% (p =0.04) respectively of the RNA levels observed in the mice injected with empty virus (Fig. 7A and B).

Finally we demonstrated that restoration of miR-378a abundance and the associated reduction in *Bmp2* and *Smad5* RNA abundances moderated aortic calcification. Exposure to the mir-378a-bearing virus reduced aortic calcium levels by a third (63 ±0.6% of empty control, p=0.02) relative to levels in mice exposed to the empty virus (Fig. 7C). Thus as observed for miR-145, forced expression of miR-378a, significantly ameliorated pathological calcification of the aorta.

Discussion

Mice generally resist cardiovascular calcification. Genetic modifications that impact lipid or mineral metabolism or high fat/high cholesterol diets or surgical models of renal failure are required to adequately mimic atherosclerosis. Some of these models are experimentally time-consuming. For example, mice with genetically sensitized hyperlipidemia backgrounds must be fed special diets for months (41,42). In contrast, *Klotho* mutant mice with hyperphosphatemia exhibit elevated BMP signaling and calcification in the aorta at 6-7 weeks of age. The swift pace of aortic calcification in the *Klotho* strain facilitates the testing of therapeutic approaches to reducing calcification. Indeed, only 10 days of exposure to viruses bearing selected miRNAs caused a statistically significant reduction in aortic calcification (Fig. 4, 7). Studies using *Klotho* mutant mice also are relevant to human biology, because KLOTHO deficiency is associated with human diseases involving soft tissue and vascular calcification such as chronic kidney disease (43-46).

We obtained and analyzed miRNA profiles in aortas from control healthy and *Klotho* homozygous mutant mice with renal impairment that causes aortic calcification. Our analyses of computationally predicted target genes and the biological processes these genes affect suggest that many regulated miRNAs influence osteogenic differentiation (Fig. 2, Supporting Fig. 1). Notably, in both sexes, the biological process of skeletal development and the WNT and HIPPO signaling pathways were associated with the differentially regulated sets of genes. Along with BMP signaling, these pathways are closely involved in the osteogenic differentiation observed in both bones and in abnormally calcified soft tissues (3,4). Our discovery of common target profiles is

consistent with the prevailing view that cardiovascular calcification proceeds by known bone formation pathways that have been ectopically activated by pathologies.

A large number of miRNAs that potentially regulate BMP signaling were identified within our profiles of differentially regulated miRNAs. We selected miR-145 and miR-378 to test the principle that miRNAs targeting several members of the BMP signaling pathway would reduce KLOTHO deficiency-associated calcification. Our gain-of-function approach, whereby a VSMC-targeted lentiviral vector bearing mir-145 or mir-378a was injected into *Klotho* mutant mice, raised the abundances of these miRNAs in mouse aorta relative to empty virus (Fig. 5). *Bmp2* and *Smad5* RNA levels in aortas from mice injected with either virus fell significantly, indicating that these miRNAs could modulate BMP signaling (Fig. 6, 7). Most importantly, *Klotho* mice injected with each miRNA-bearing virus had one third lower aortic calcium relative to mice injected with empty virus (Fig. 6, 7). Consistent with our results, forced overexpression of miR-145 decreased atherosclerotic plaque size, increased plaque stability, and promoted a contractile cell phenotype in the *ApoE*, high fat diet mouse model of hyperlipidemia (38). Our proof-of-principle experiments confirm that the strategy of manipulating miRNA levels *in vivo* can ameliorate the elevated BMP signaling and calcification associated with pro-calcific diseases.

In summary, we have provided a database of the miRNAs that are differentially expressed in healthy mouse aorta relative to aorta calcified due to defective mineral metabolism and kidney function. We also demonstrated that forced expression of miR-145 and miR-378 inhibited *Bmp2* and *Smad5* RNA levels. MiR-RNA-145 and miR-378

are candidates for translational studies investigating therapies to block vascular calcification.

References

1. Benjamin, E. J., Muntner, P., Alonso, A., Bittencourt, M. S., Callaway, C. W., Carson, A. P., Chamberlain, A. M., Chang, A. R., Cheng, S., Das, S. R., Delling, F. N., Djousse, L., Elkind, M. S. V., Ferguson, J. F., Fornage, M., Jordan, L. C., Khan, S. S., Kissela, B. M., Knutson, K. L., Kwan, T. W., Lackland, D. T., Lewis, T. T., Lichtman, J. H., Longenecker, C. T., Loop, M. S., Lutsey, P. L., Martin, S. S., Matsushita, K., Moran, A. E., Mussolino, M. E., O'Flaherty, M., Pandey, A., Perak, A. M., Rosamond, W. D., Roth, G. A., Sampson, U. K. A., Satou, G. M., Schroeder, E. B., Shah, S. H., Spartano, N. L., Stokes, A., Tirschwell, D. L., Tsao, C. W., Turakhia, M. P., VanWagner, L. B., Wilkins, J. T., Wong, S. S., Virani, S. S., American Heart Association Council on, E., Prevention Statistics, C., and Stroke Statistics, S. (2019) Heart Disease and Stroke Statistics-2019 Update: A Report From the American Heart Association. *Circulation* **139**, e56-e528
2. Karwowski, W., Naumnik, B., Szczepanski, M., and Mysliwiec, M. (2012) The mechanism of vascular calcification - a systematic review. *Med Sci Monit* **18**, RA1-11
3. Yutzey, K. E., Demer, L. L., Body, S. C., Huggins, G. S., Towler, D. A., Giachelli, C. M., Hofmann-Bowman, M. A., Mortlock, D. P., Rogers, M. B., Sadeghi, M. M., and Aikawa, E. (2014) Calcific aortic valve disease: a consensus summary from the Alliance of Investigators on Calcific Aortic Valve Disease. *Arterioscler Thromb Vasc Biol* **34**, 2387-2393
4. Towler, D. A. (2017) Commonalities Between Vasculature and Bone An Osseocentric View of Arteriosclerosis. *Circulation* **135**, 320-322
5. Bostrom, K., Watson, K. E., Horn, S., Wortham, C., Herman, I. M., and Demer, L. L. (1993) Bone morphogenetic protein expression in human atherosclerotic lesions. *J Clin Invest* **91**, 1800-1809
6. Nagy, E., Eriksson, P., Yousry, M., Caidahl, K., Ingelsson, E., Hansson, G. K., Franco-Cereceda, A., and Back, M. (2013) Valvular osteoclasts in calcification and aortic valve stenosis severity. *Int J Cardiol* **168**, 2264-2271
7. Yang, X., Meng, X., Su, X., Mauchley, D. C., Ao, L., Cleveland, J. C., Jr., and Fullerton, D. A. (2009) Bone morphogenic protein 2 induces Runx2 and osteopontin expression in human aortic valve interstitial cells: role of Smad1 and extracellular signal-regulated kinase 1/2. *J Thorac Cardiovasc Surg* **138**, 1008-1015
8. Cheng, S. L., Shao, J. S., Charlton-Kachigian, N., Loewy, A. P., and Towler, D. A. (2003) MSX2 promotes osteogenesis and suppresses adipogenic

differentiation of multipotent mesenchymal progenitors. *J Biol Chem* **278**, 45969-45977

9. Yu, Z., Seya, K., Daitoku, K., Motomura, S., Fukuda, I., and Furukawa, K. (2011) Tumor necrosis factor-alpha accelerates the calcification of human aortic valve interstitial cells obtained from patients with calcific aortic valve stenosis via the BMP2-Dlx5 pathway. *J Pharmacol Exp Ther* **337**, 16-23
10. Osman, L., Yacoub, M. H., Latif, N., Amrani, M., and Chester, A. H. (2006) Role of human valve interstitial cells in valve calcification and their response to atorvastatin. *Circulation* **114**, I547-552
11. Nigam, V., and Srivastava, D. (2009) Notch1 represses osteogenic pathways in aortic valve cells. *J Mol Cell Cardiol* **47**, 828-834
12. Wirrig, E. E., Hinton, R. B., and Yutzey, K. E. (2011) Differential expression of cartilage and bone-related proteins in pediatric and adult diseased aortic valves. *J Mol Cell Cardiol* **50**, 561-569
13. Miller, J. D., Weiss, R. M., Serrano, K. M., Castaneda, L. E., Brooks, R. M., Zimmerman, K., and Heistad, D. D. (2010) Evidence for active regulation of pro-osteogenic signaling in advanced aortic valve disease. *Arterioscler Thromb Vasc Biol* **30**, 2482-2486
14. Mohler, E. R., 3rd, Gannon, F., Reynolds, C., Zimmerman, R., Keane, M. G., and Kaplan, F. S. (2001) Bone formation and inflammation in cardiac valves. *Circulation* **103**, 1522-1528
15. Nakagawa, Y., Ikeda, K., Akakabe, Y., Koide, M., Uraoka, M., Yutaka, K. T., Kurimoto-Nakano, R., Takahashi, T., Matoba, S., Yamada, H., Okigaki, M., and Matsubara, H. (2010) Paracrine osteogenic signals via bone morphogenetic protein-2 accelerate the atherosclerotic intimal calcification in vivo. *Arterioscler Thromb Vasc Biol* **30**, 1908-1915
16. Gomez-Stallons, M. V., Wirrig-Schwendeman, E. E., Hassel, K. R., Conway, S. J., and Yutzey, K. E. (2016) Bone Morphogenetic Protein Signaling Is Required for Aortic Valve Calcification. *Arterioscler Thromb Vasc Biol* **36**, 1398-1405
17. Balachandran, K., Sucosky, P., Jo, H., and Yoganathan, A. P. (2010) Elevated cyclic stretch induces aortic valve calcification in a bone morphogenic protein-dependent manner. *Am J Pathol* **177**, 49-57
18. Derwall, M., Malhotra, R., Lai, C. S., Beppu, Y., Aikawa, E., Seehra, J. S., Zapol, W. M., Bloch, K. D., and Yu, P. B. (2012) Inhibition of bone morphogenetic protein signaling reduces vascular calcification and atherosclerosis. *Arterioscler Thromb Vasc Biol* **32**, 613-622
19. Malhotra, R., Burke, M. F., Martyn, T., Shakartzi, H. R., Thayer, T. E., O'Rourke, C., Li, P., Derwall, M., Spagnolli, E., Kolodziej, S. A., Hoeft, K., Mayeur, C., Jiramongkolchai, P., Kumar, R., Buys, E. S., Yu, P. B., Bloch, K. D., and Bloch, D. B. (2015) Inhibition of bone morphogenetic protein signal transduction prevents the medial vascular calcification associated with matrix Gla protein deficiency. *PLoS One* **10**, e0117098
20. Corbett, A. H. (2018) Post-transcriptional regulation of gene expression and human disease. *Curr Opin Cell Biol* **52**, 96-104

21. Fotinos, A., Fritz, D. T., Lisica, S., Liu, Y., and Rogers, M. B. (2016) Competing Repressive Factors Control Bone Morphogenetic Protein 2 (BMP2) in Mesenchymal Cells. *J Cell Biochem* **117**, 439-447
22. Rogers, M. B., Shah, T. A., and Shaikh, N. N. (2015) Turning Bone Morphogenetic Protein 2 (BMP2) on and off in Mesenchymal Cells. *J Cell Biochem* **116**, 2127-2138
23. Shah, T. A., Zhu, Y., Shaikh, N. N., Harris, M. A., Harris, S. E., and Rogers, M. B. (2017) Characterization of new bone morphogenetic protein (Bmp)-2 regulatory alleles. *Genesis* **55**
24. Kuro-o, M., Matsumura, Y., Aizawa, H., Kawaguchi, H., Suga, T., Utsugi, T., Ohyama, Y., Kurabayashi, M., Kaname, T., Kume, E., Iwasaki, H., Iida, A., Shiraki-Iida, T., Nishikawa, S., Nagai, R., and Nabeshima, Y. I. (1997) Mutation of the mouse klotho gene leads to a syndrome resembling ageing. *Nature* **390**, 45-51
25. Hu, M. C., Shi, M., Zhang, J., Quinones, H., Griffith, C., Kuro-o, M., and Moe, O. W. (2011) Klotho deficiency causes vascular calcification in chronic kidney disease. *J Am Soc Nephrol* **22**, 124-136
26. Yamada, S., and Giachelli, C. M. (2017) Vascular calcification in CKD-MBD: Roles for phosphate, FGF23, and Klotho. *Bone* **100**, 87-93
27. Shah, T. A. (2018) *Post-transcriptional Gene Regulation of Bone Morphogenetic Protein (BMP)-2 During Embryogenesis and Cardiovascular Calcification.* Ph.D., Rutgers School of Graduate Studies
28. Shah, T. A., Tang, Y., Yurkow, E. J., and Rogers, M. B. (2019) Post-Transcriptional Bone Morphogenetic Protein 2 (BMP2) Gene Regulation in Aorta. (https://www.biorxiv.org/ ed., BIORXIV/2019/735852
29. Paraskevopoulou, M. D., Georgakilas, G., Kostoulas, N., Vlachos, I. S., Vergoulis, T., Reczko, M., Filippidis, C., Dalamagas, T., and Hatzigeorgiou, A. G. (2013) DIANA-microT web server v5.0: service integration into miRNA functional analysis workflows. *Nucleic Acids Res* **41**, W169-173
30. Yu, G., Wang, L. G., Han, Y., and He, Q. Y. (2012) clusterProfiler: an R package for comparing biological themes among gene clusters. *OMICS* **16**, 284-287
31. Betel, D., Wilson, M., Gabow, A., Marks, D. S., and Sander, C. (2008) The microRNA.org resource: targets and expression. *Nucleic Acids Res* **36**, D149-153
32. Shannon, P., Markiel, A., Ozier, O., Baliga, N. S., Wang, J. T., Ramage, D., Amin, N., Schwikowski, B., and Ideker, T. (2003) Cytoscape: a software environment for integrated models of biomolecular interaction networks. *Genome Res* **13**, 2498-2504
33. Johnson, J. L. (2019) Elucidating the contributory role of microRNA to cardiovascular diseases (a review). *Vascul Pharmacol* **114**, 31-48
34. Garcia de Vinuesa, A., Abdelilah-Seyfried, S., Knaus, P., Zwijsen, A., and Bailly, S. (2016) BMP signaling in vascular biology and dysfunction. *Cytokine Growth Factor Rev* **27**, 65-79
35. Bostrom, K. I., Rajamannan, N. M., and Towler, D. A. (2011) The regulation of valvular and vascular sclerosis by osteogenic morphogens. *Circ Res* **109**, 564-577

36. Leopold, J. A. (2012) Cellular mechanisms of aortic valve calcification. *Circ Cardiovasc Interv* **5**, 605-614
37. Vacante, F., Denby, L., Sluimer, J. C., and Baker, A. H. (2019) The function of miR-143, miR-145 and the MiR-143 host gene in cardiovascular development and disease. *Vascul Pharmacol* **112**, 24-30
38. Lovren, F., Pan, Y., Quan, A., Singh, K. K., Shukla, P. C., Gupta, N., Steer, B. M., Ingram, A. J., Gupta, M., Al-Omran, M., Teoh, H., Marsden, P. A., and Verma, S. (2012) MicroRNA-145 targeted therapy reduces atherosclerosis. *Circulation* **126**, S81-90
39. Yang, Y. J., Luo, S., and Wang, L. S. (2019) Effects of microRNA-378 on epithelial-mesenchymal transition, migration, invasion and prognosis in gastric carcinoma by targeting BMP2. *Eur Rev Med Pharmacol Sci* **23**, 5176-5186
40. Hou, X., Tang, Z., Liu, H., Wang, N., Ju, H., and Li, K. (2012) Discovery of MicroRNAs associated with myogenesis by deep sequencing of serial developmental skeletal muscles in pigs. *PLoS One* **7**, e52123
41. Neven, E., and D'Haese, P. C. (2011) Vascular calcification in chronic renal failure: what have we learned from animal studies? *Circ Res* **108**, 249-264
42. Miller, J. D., Weiss, R. M., and Heistad, D. D. (2011) Calcific aortic valve stenosis: methods, models, and mechanisms. *Circ Res* **108**, 1392-1412
43. Koh, N., Fujimori, T., Nishiguchi, S., Tamori, A., Shiomi, S., Nakatani, T., Sugimura, K., Kishimoto, T., Kinoshita, S., Kuroki, T., and Nabeshima, Y. (2001) Severely reduced production of klotho in human chronic renal failure kidney. *Biochem Biophys Res Commun* **280**, 1015-1020
44. Ichikawa, S., Imel, E. A., Kreiter, M. L., Yu, X., Mackenzie, D. S., Sorenson, A. H., Goetz, R., Mohammadi, M., White, K. E., and Econs, M. J. (2007) A homozygous missense mutation in human KLOTHO causes severe tumoral calcinosis. *J Clin Invest* **117**, 2684-2691
45. Arking, D. E., Atzmon, G., Arking, A., Barzilai, N., and Dietz, H. C. (2005) Association between a functional variant of the KLOTHO gene and high-density lipoprotein cholesterol, blood pressure, stroke, and longevity. *Circ Res* **96**, 412-418
46. Arking, D. E., Becker, D. M., Yanek, L. R., Fallin, D., Judge, D. P., Moy, T. F., Becker, L. C., and Dietz, H. C. (2003) KLOTHO allele status and the risk of early-onset occult coronary artery disease. *Am J Hum Genet* **72**, 1154-1161

Fig. 1. MiRNA profiles in the aorta from control (CTR) and *Klotho homozygous (KK)* mutant mice. Aortas were isolated from control (**CTR**) mice bearing the wild type (Wt) or heterozygous (*+/Kl*) *Klotho* genotypes, or diseased (**KK**) homozygous (*Kl/Kl*) *Klotho* mice between 40 and 50 days of age. Control mice were healthy with normal kidney function. *Klotho* mutant homozygous mice had pathologically calcified aorta. RNA was extracted and samples were assayed using Affymetrix miRNA version 4.0. Data analysis was performed after Robust Multi-Array Average (RMA) normalization with the Partek Genomics Suite 7.0. Heat maps illustrate miRNAs whose abundances differed significantly in aorta from control mice or diseased mice ($p < 0.05$). Green color indicates a low relative expression level, and red indicates a high relative expression level.

MicroRNA profiles in calcified *vs*. healthy aorta

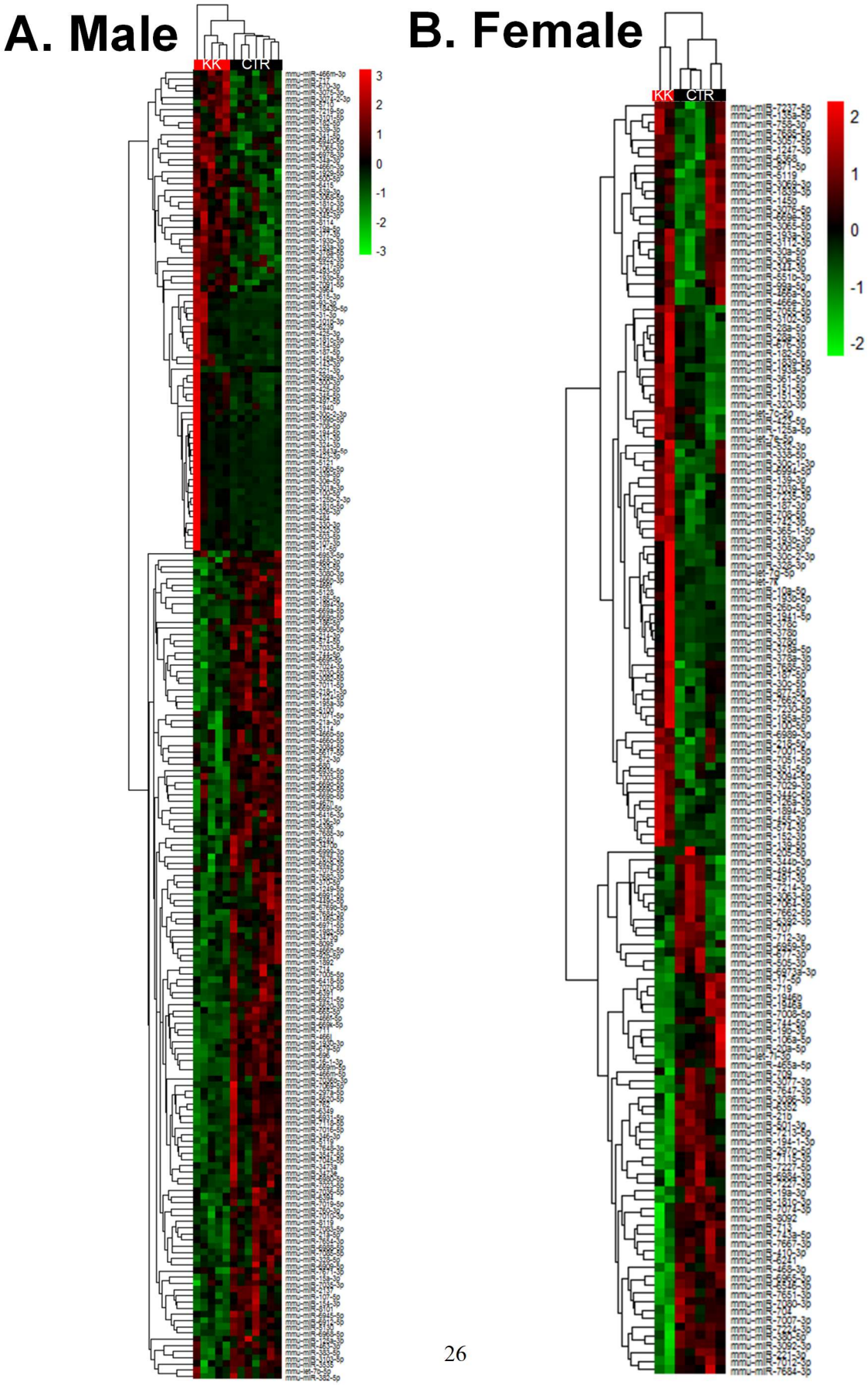

Fig. 2. Gene Ontology (GO) analyses of differentially regulated miRNAs. The genes potentially targeted by differentially expressed miRNAs were predicted by DIANA TOOLS. Target genes were grouped into gene ontology biologic process terms using the Gene Ontology database and R software. The x-axis represents the number of genes associated with each gene ontology biologic process term. Low p adjust values are in red and high p adjust values are in blue. GO terms that are directly related to the osteogenic differentiation that occurs in vascular calcification are marked with an asterisk (*).

MicroRNA profiles in calcified *vs*. healthy aorta

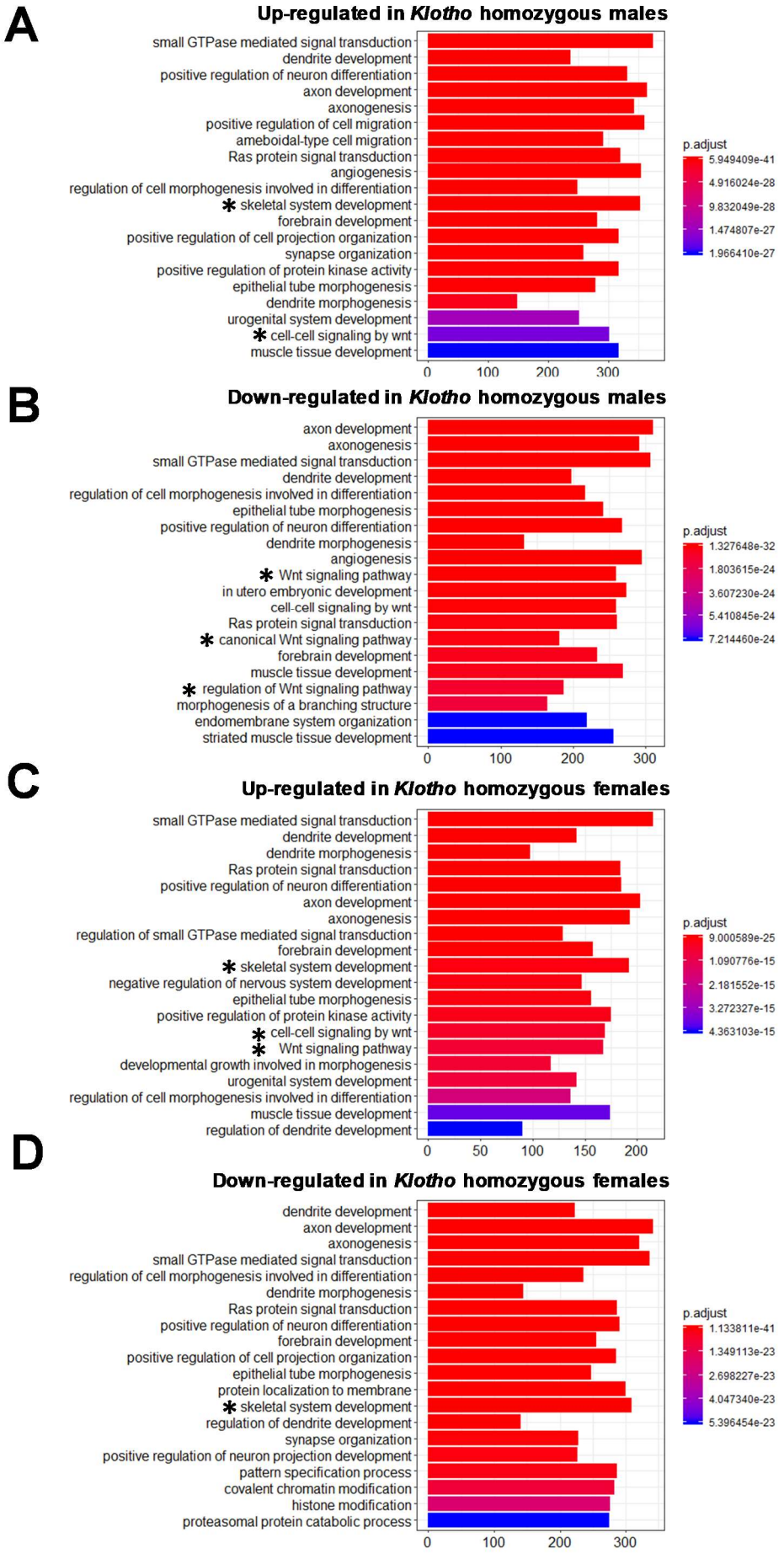

Fig. 3. Interaction network of miRNAs down-regulated in *Klotho* homozygotes relative to healthy controls. Boxed miRNAs on top are predicted to target *Bmp2* and two or three downstream BMP signaling intermediaries, *Smads1, 5, 9*. Boxed miRNAs on bottom are decreased by 50% or more in both male and female *Klotho* homozygotes and target 1 or more of these protein-coding transcripts. Lentiviral delivery of the bold-faced, underlined RNAs has been shown to reduce calcification (Fig. 6, 7).

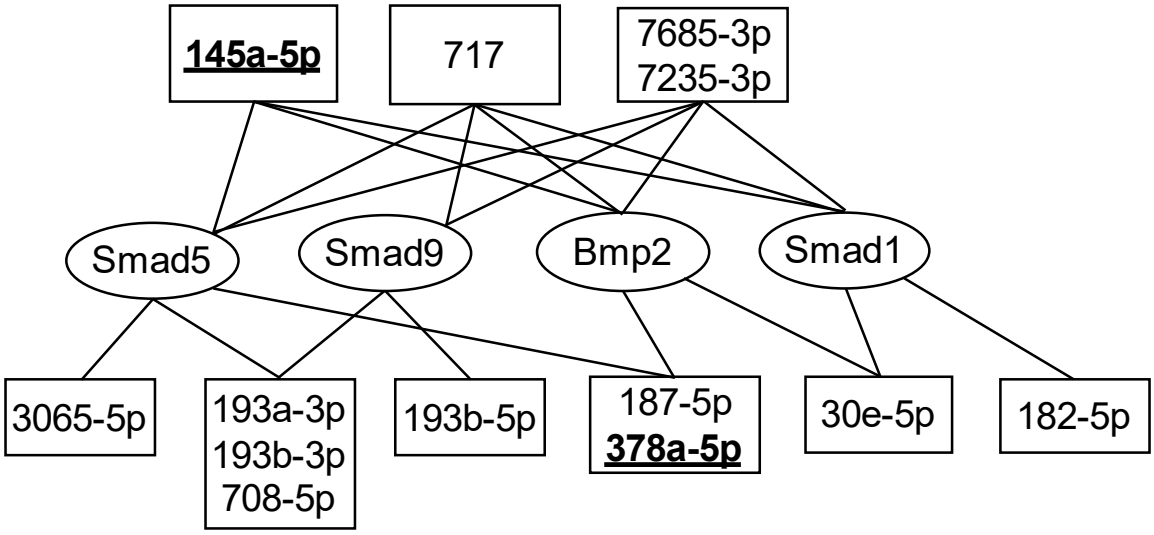

Fig. 4. MiR-145 and miR-378a abundance is reduced in *Klotho* homozygous mutant mice (KK). Relative miRNA levels in healthy controls ($Kl^{+/+}$ and $Kl^{kl/+}$) or *Klotho* homozygous ($Kl^{kl/kl}$) mice (**KK**) were assessed by Affymetrix microarrays (**A, C, E**) as described earlier or by RT PCR normalized against the corresponding U6 expression (**B, D, F**). The bars represent the mean value +/- SEM and solid and hollow circles represent individual male and female values, respectively. * = $p < 0.05$, ** = $p < 0.01$.

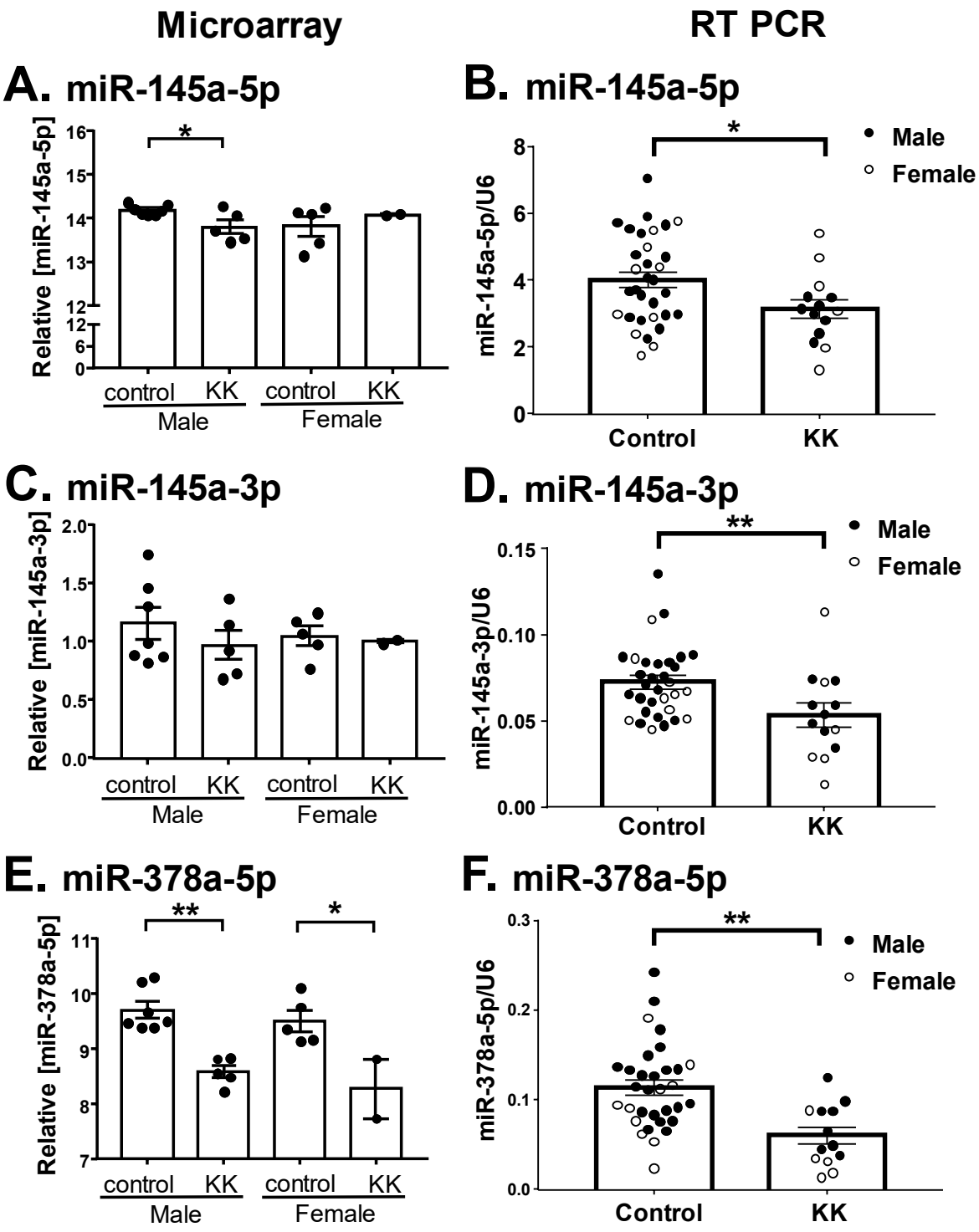

Fig. 5. Vascular smooth muscle cell (VSMC)-specific lentivirus treatment increases mir-145 and mir-378a abundance in *Klotho* mutant mice. (A) Weaned *Klotho* mutant homozygous mice were treated with empty virus or virus bearing miR-145 or miR-378a pre-miRNAs. The miR-145a-5p **(B)**, miR-145a-3p **(C)** and miR-378a-5p abundances were evaluated by real-time PCR and normalized against the corresponding U6 abundance. The bars represent the mean value +/- SEM. Solid and hollow circles represent individual male and female values, respectively. ** = $p < 0.01$.

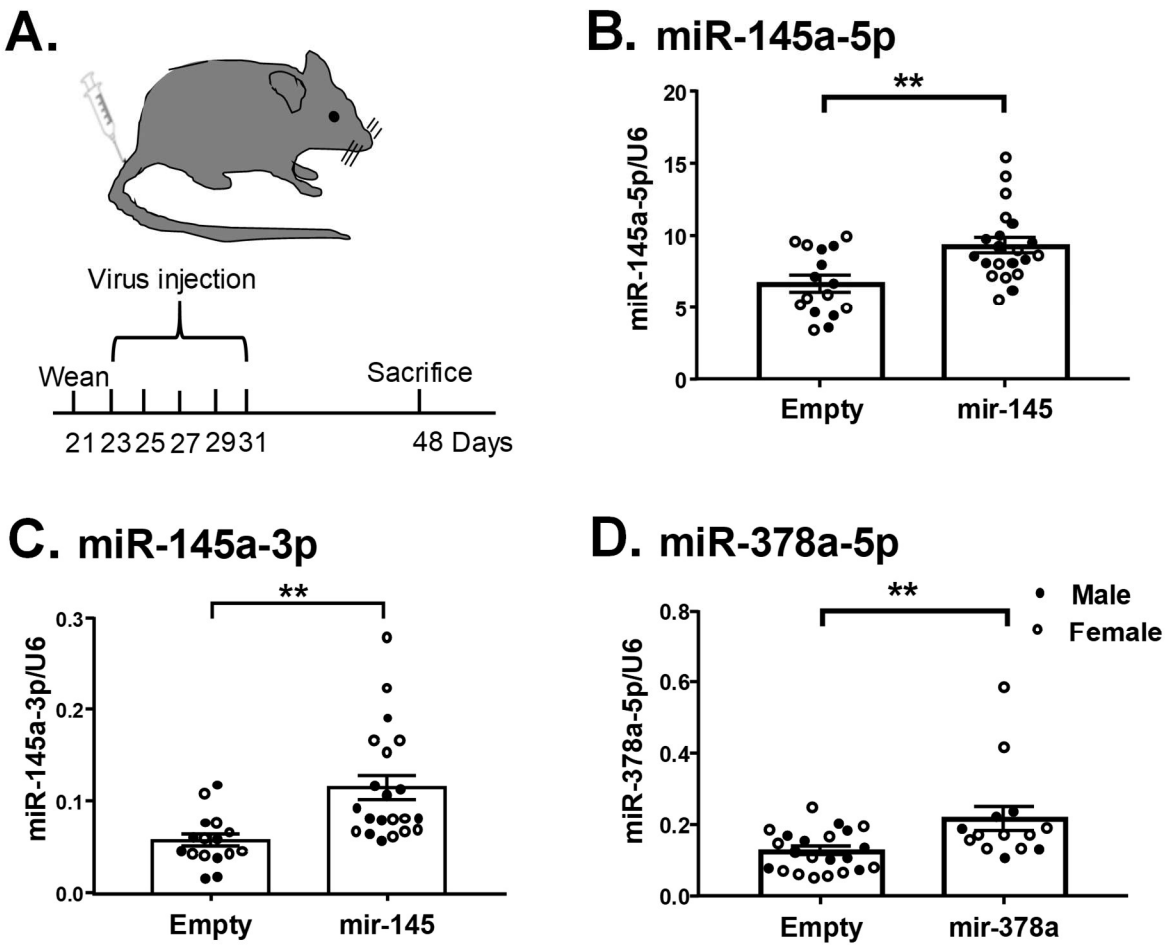

Fig. 6. Restoring MiR-145 levels reduces the abundance of RNAs encoding BMP signaling factors and aortic calcification. Increased mir-145 abundance in *Klotho* mutant mice significantly decreased *Bmp2* **(A)** and *Smad5* **(C)** RNA levels and calcium levels **(D)**. *Smad1* **(B)** RNA levels did not change. The bars represent the mean value +/- SEM. Solid and hollow circles represent individual male and female values, respectively. * = $p < 0.05$, ** = $p < 0.01$.

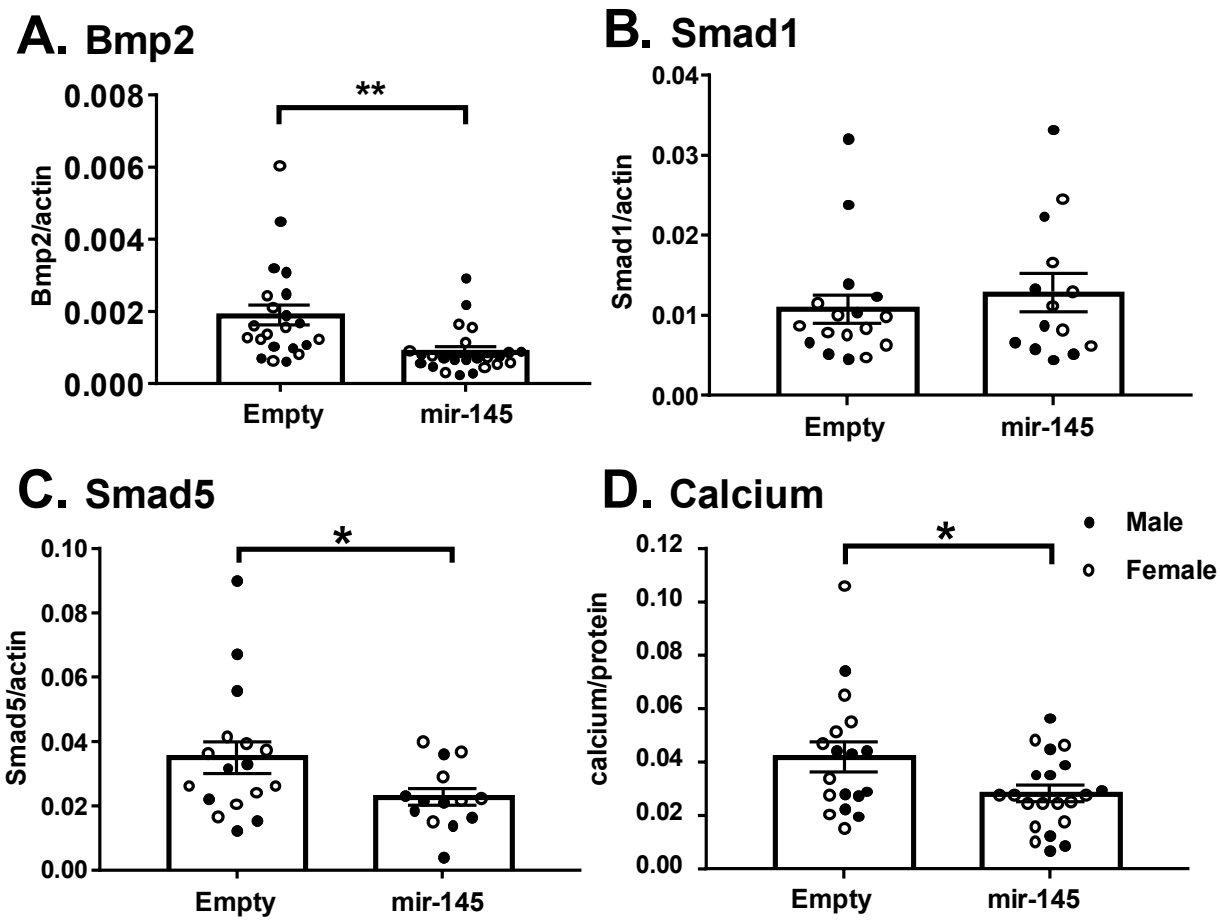

Fig. 7. Restoring MiR-378a levels reduces the abundance of RNAs encoding BMP signaling factors and aortic calcification. Increased mir-378a abundance in *klotho* mutant mice significantly decreased *Bmp2* **(A)**, *Smad5* **(B)** RNA and calcium levels **(C)**. The bars represent the mean value +/- SEM. Solid and hollow circles represent individual male and female values, respectively. * = $p < 0.05$.

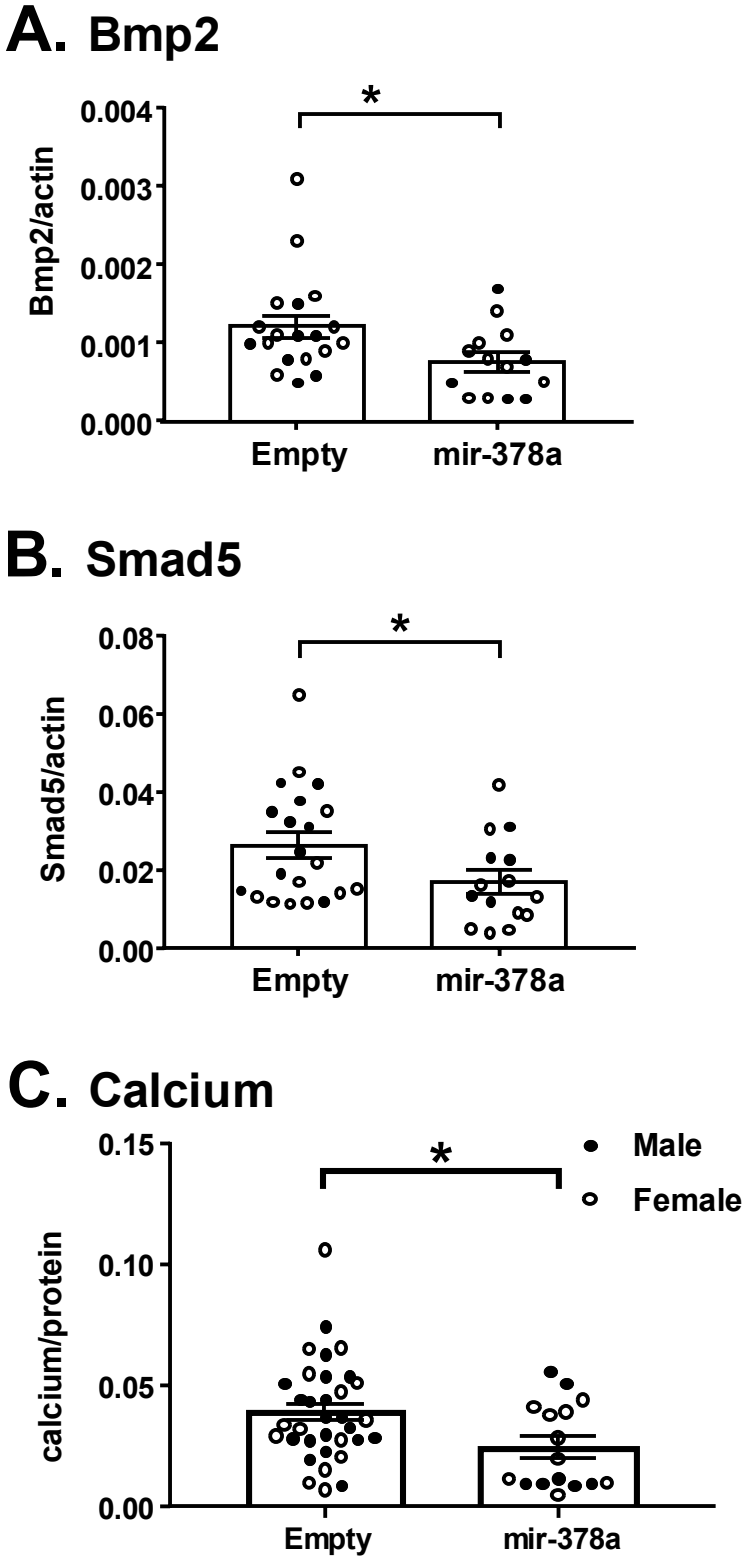

Supporting Fig. 1. KEGG (Kyoto Encyclopedia of Genes and Genomes) analyses of differentially regulated miRNAs. The genes potentially targeted by differentially expressed miRNAs were predicted by DIANA TOOLS. These genes were grouped into gene pathways with the KEGG database and R software. The y-axis represents the names of the top 20 KEGG enriched pathways. The x-axis represents the Gene Ratio which is the ratio of the gene number in each pathway to the total gene number. Low p adjust values are in red and high p adjust values are in blue. The size of each circle is proportional to the number of enriched genes. KEGG terms that are directly related to the osteogenic differentiation that occurs in vascular calcification are marked with an asterisk (*).

A

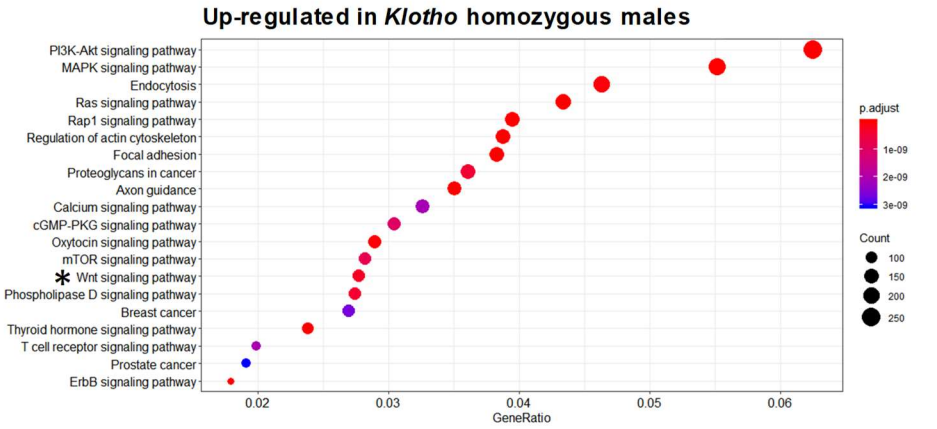

B

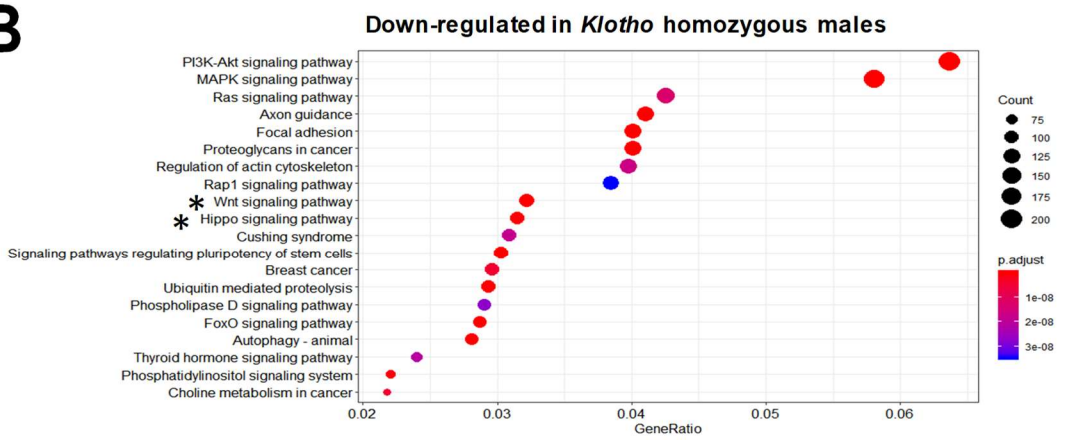

C

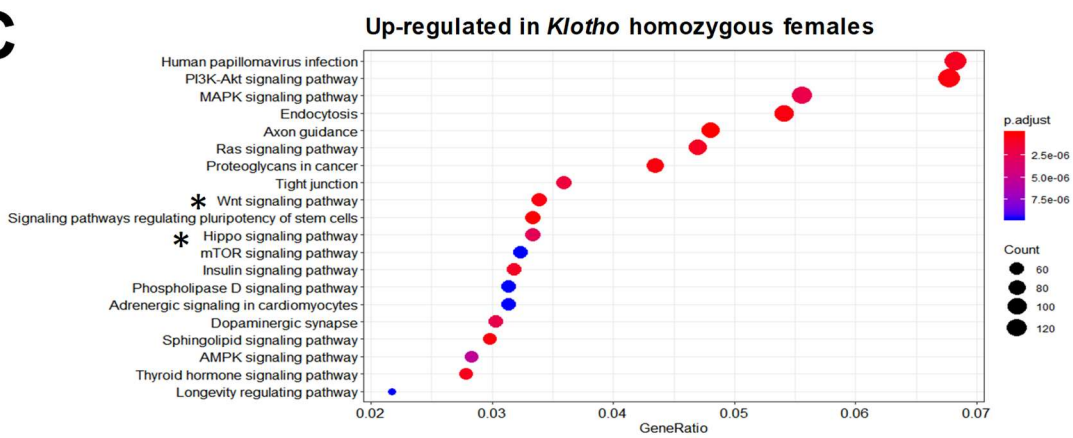

D

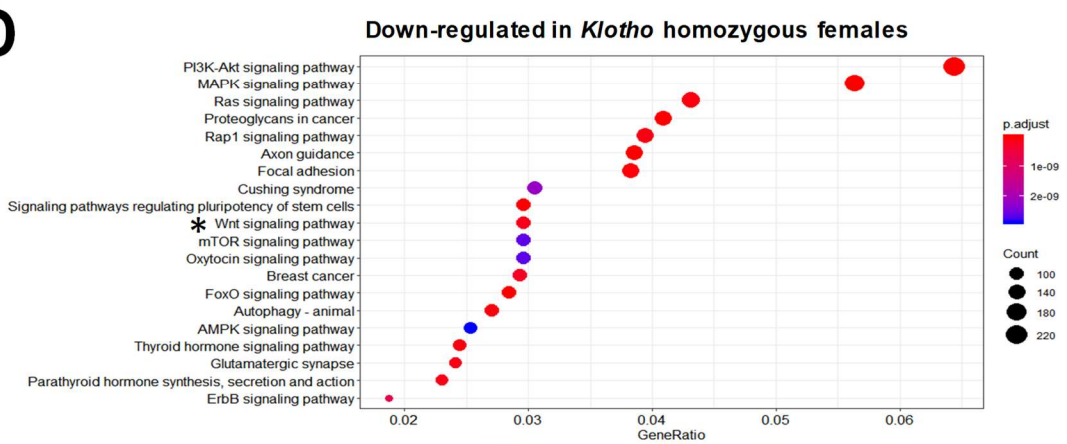

Supporting Fig. 2. Interaction network of miRNAs down-regulated in *Klotho* homozygous males relative to healthy controls. The indicated miRNAs were down-regulated in diseased *Klotho* mice according to microarray or RT-PCR assays and also are predicted to target *Bmp2* and/or the downstream BMP signaling intermediaries, *Smads1, 5, 9*. Bold face and underlining labels the miRNAs whose abundance decreased in both male and female *Klotho* homozygotes.

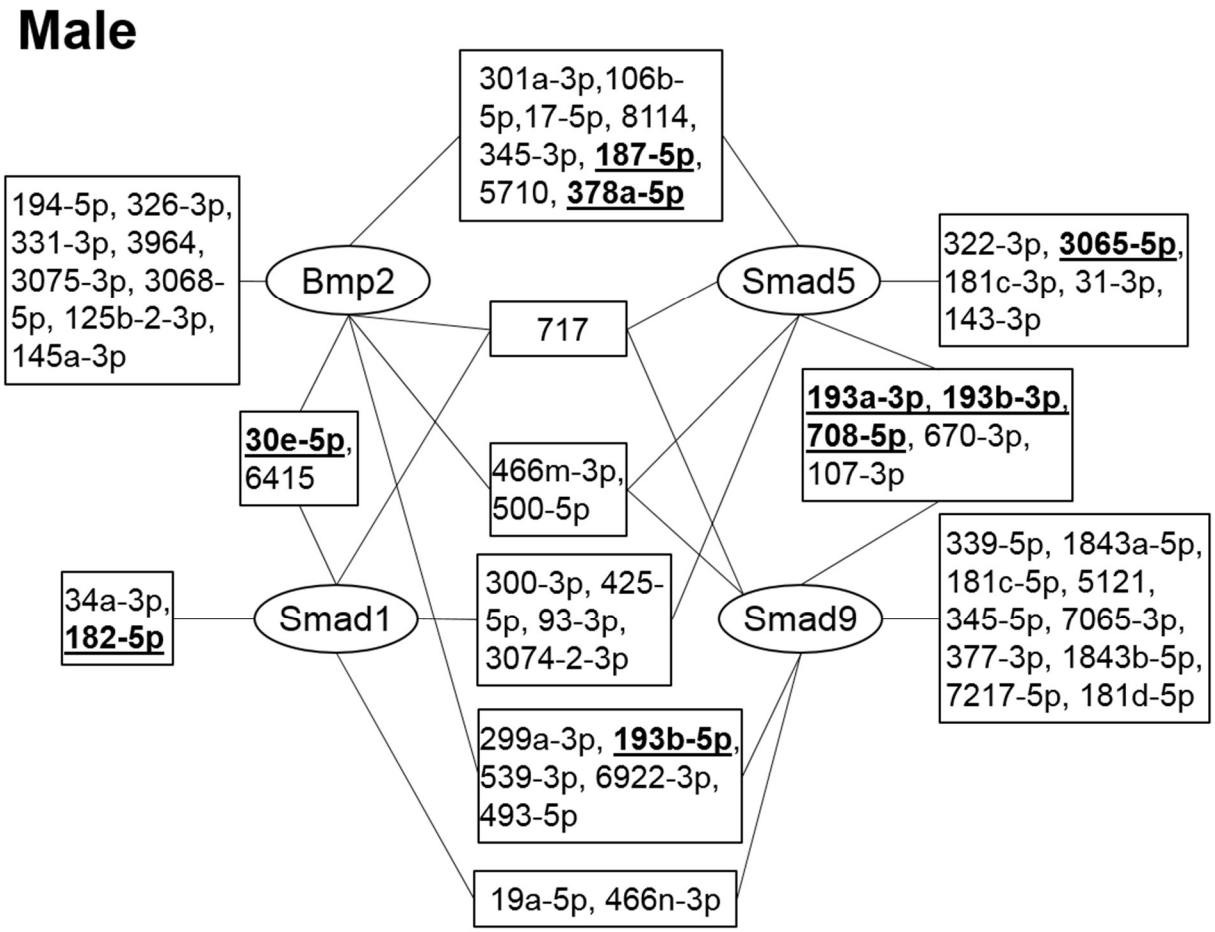

Supporting Fig. 3. Interaction network of miRNAs down-regulated in *Klotho* homozygous females relative to healthy controls. The indicated miRNAs were down-regulated in diseased Klotho mice according to microarray or RT-PCR assays and also are predicted to target *Bmp2* and/or the downstream BMP signaling intermediaries, *Smads1, 5, 9*. Target genes are in ovals. Bold face and underlining labels the miRNAs whose abundance decreased in both male and female *Klotho* homozygotes.

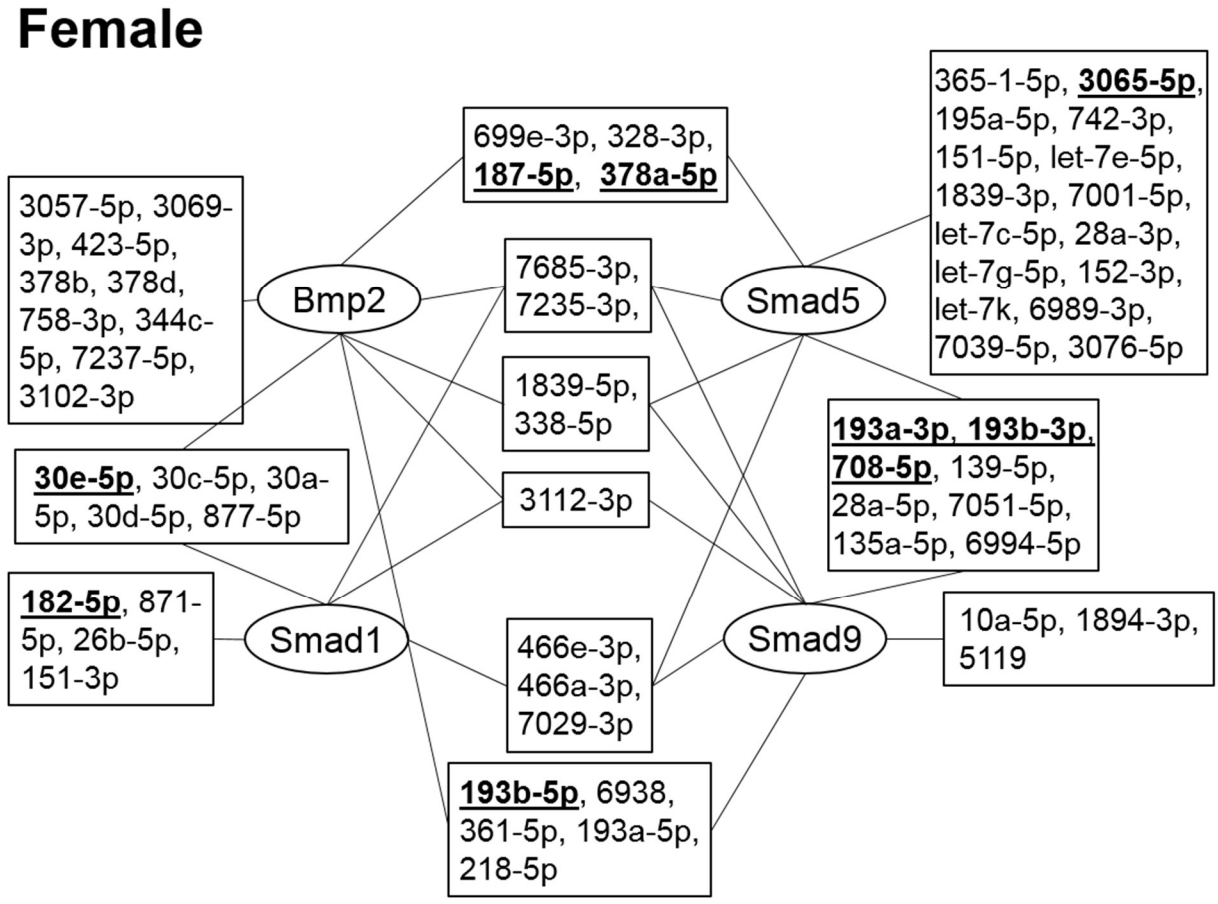

Supporting Table 1.

MicroRNA abundance in aorta from *Klotho* mutant homozygotes relative to healthy control. The percentage change for each miRNA whose abundance was significantly changed ($p < 0.5$) between *Klotho* homozygotes and control mice was calculated by the Partek Genomics Suite 7.0 (Partek Inc., St. Louis, MO).